

The generation of high-quality, intense ion beams by ultra-intense lasers

M Roth¹, M Allen², P Audebert³, A Blazevic¹, E Brambrink¹,
T E Cowan², J Fuchs³, J-C Gauthier³, M Geißel¹, M Hegelich⁴,
S Karsch⁴, J Meyer-ter-Vehn⁴, H Ruhl², T Schlegel¹ and R B Stephens²

¹ Gesellschaft für Schwerionenforschung mbH, Planckstr. 1, 64291 Darmstadt, Germany

² General Atomics, PO Box 85608, San Diego, CA 92186-5608, USA

³ Laboratoire pour l'Utilisation des Lasers Intenses, 91128 Palaiseau, France

⁴ Max-Planck-Institut für Quantenoptik, Garching, Germany

Received 12 September 2002

Published 21 November 2002

Online at stacks.iop.org/PPCF/44/B99

Abstract

Intense beams of protons and heavy ions have been observed in ultra-intense laser–solid interaction experiments. Thereby, a considerable fraction of the laser energy is transferred to collimated beams of energetic ions (e.g. up to 50 MeV protons; 100 MeV fluorine), which makes these beams highly interesting for various applications. Experimental results indicate a very short-pulse duration and an excellent beam quality, leading to beam intensities in the TW range. To characterize the beam quality and its dependence on laser parameters and target conditions we performed experiments using the 100 TW laser system at Laboratoire pour l'Utilisation des Lasers Intenses at the Ecole Polytechnique, France, with focused intensities exceeding 10^{19} W cm⁻². We found a strong dependence on the target rear surface conditions allowing to tailor the ion beam by an appropriate target design. We also succeeded in the generation of heavy ion beams by suppressing the proton amount at the target surface.

We will present recent experimental results demonstrating a transverse beam emittance far superior to the accelerator based ion beams. Finally, we will discuss the prospect of laser accelerated ion beams as new diagnostics in laser–solid interaction experiments. Special fields of interest are proton radiography, electric field imaging, and relativistic electron transport inside the target.

1. Introduction

Energetic ions have been produced by lasers focused onto solid targets for several decades. The predominant mechanism in those experiments was found to be an isothermal expansion

with ions being fed into the expanding corona by a rarefaction wave propagating at the sound speed, c_s , into the bulk plasma. In these experiments ions, mostly originating from the target front, moved against the laser direction and showed a very large dispersion. Typical energies were of the order of 100 keV/nucleon for sub-kJ lasers and up to 2 MeV for protons from kJ systems. With the advent of ultra-intense, short-pulse lasers the situation changed dramatically. Nowadays even table-top, low energy laser systems produce protons up to several MeV particle energy and collimated beams of ions have been observed [1, 2].

Ion emission has been observed originating from the front and rear surface of solid targets. In contrast to the experiments using long-pulse lasers, ions accelerated by fs-laser systems are emitted normal to the rear surface in a low divergent beam of excellent quality. The dominant mechanism of the ion acceleration is understood as rear surface emission accelerated by the target normal sheath acceleration (TNSA) mechanism [3]. Relativistic electrons generated from the laser–plasma interaction, having an average temperature of several MeV, envelope the target foil and form an electron plasma sheath on the rear, non-irradiated surface. The electric field in the sheath ($E_{\text{stat}} \sim kT_{\text{hot}}/e\lambda_D$, $\lambda_D = (\epsilon_0 kT_{\text{hot}}/e^2 n_{e,\text{hot}})^{1/2}$) can reach $>10^{12}$ V m⁻¹. A few monolayers of atoms at the rear surface are field-ionized and accelerated normal to the surface by E_{stat} , with the most energetic electrons always extending further out into vacuum, maintaining the accelerating field as long as the electron temperature is high. This is fundamentally different from the long-pulse case, in which bulk effects and collisional ionization by thermal electrons in the coronal plasma are the dominant mechanisms. So far mainly protons have been observed from the rear side, originating, as in the long-pulse experiments, from contaminating hydrocarbon layers which coat the targets. As soon as protons are present they outrun the heavier ions due to their superior charge-to-mass ratio, and screen the acceleration field. Thus protons are preferentially accelerated in favour of heavier ions over a distance of a few microns, and up to tens of MeV. This forms a collimated beam with an approximately exponential energy distribution with 5–6 MeV. The conversion efficiency from laser energy to ion beam energy can be quite high and efficiencies of order of 10% have already been measured [2]. This acceleration mechanism makes these intense ion beams highly interesting for many applications [4–6], especially if one can collimate or focus the beam by shaping the target, as suggested by numerical calculations [7, 8]. Because of the dependence of the ion beam on the formation of the electron sheath, this process should also reveal information about the electron transport through the target. We expect details of the ion acceleration will furthermore depend on the target material and surface conditions. Therefore, we carried out experiments to investigate the influence of these target parameters on the ion beam production.

2. Experiments

The experiments presented in this paper were performed with the 100 TW laser at Laboratoire pour l'Utilisation des Lasers Intenses (LULI). Pulses of up to 30 J at 300 fs pulse duration at $\lambda = 1.05 \mu\text{m}$ were focused with an $f/3$ off-axis parabolic mirror onto free standing target foils at normal incidence, at intensities up to 5×10^{19} W cm⁻². The focal spot diameter (FWHM) measured in vacuum was about 8 μm . Amplified spontaneous emission occurred 2 ns before the main pulse at a level of 10^{-7} of the main pulse energy and preformed a plasma.

The diagnostic setup is depicted in figure 1. The free standing target was probed by a frequency doubled laser beam parallel to the surface to determine the plasma conditions on the front and rear surface. A stack of radiochromic film (RCF) was positioned a few cm behind the target to measure the spatial beam profile. Due to the pronounced energy loss of ions at the end of their range (Bragg-peak) different layers of the RC film pack allow the imaging of the

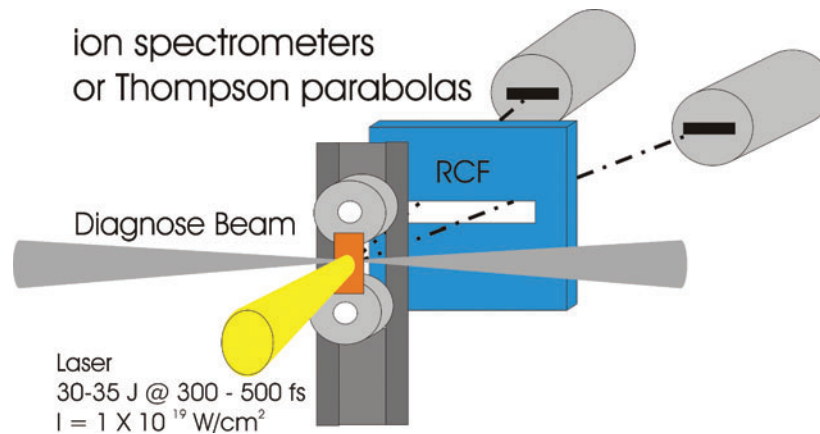


Figure 1. Experimental setup. The free standing target is irradiated at normal incidence. A slit in the RCF gives a line of sight for the particle spectrometer.

ion beam at different energies. A slot in the centre of the RCF allowed a free line of sight for the charged-particle spectrometers fielded at 0° , 6° and 13° to provide the energy distribution of the emitted electrons and ions.

Two absolutely calibrated, permanent magnetic ion spectrometers were mounted at a distance of about 1m from the target covering a solid angle of 5×10^{-6} sr.

As a complementary detector system we used titanium catcher foils, which were placed in the path of the proton beam. The ^{48}Ti is transmuted by a (p, n) reaction by protons above a sharp reaction threshold at ~ 5 MeV to an excited state of the ^{48}V isotope. Using a low-background Ge detector we observed the gamma deexcitation lines of the $^{48}\text{Ti}(p, n)^{48}\text{V}$ reaction, which provided the total activation and therefore the yield of protons above the reaction threshold of ~ 5 MeV.

To detect heavy ions accelerated from the rear surface of the relativistic-laser illuminated targets, we substituted two high resolution Thompson parabolas in replacement of one of the charged-particle spectrometers. The parallel electric and magnetic fields in the Thompson parabolas discriminated ions with respect to their momentum and charge-to-mass ratio, at the plane of the CR-39 track detectors. Careful analysis of the scanned CR-39 detectors then provides absolute numbers of the ions with respect to their kinetic energy and charge state. In addition to the ion and laser beam detectors, a silver activation neutron detector was fielded close to the target chamber determining the neutron yield for the different experiments.

Details about the experimental setup and the various detector systems were published in [5].

3. Results

3.1. Ion beam properties

We performed a series of experiments to examine the properties of the laser accelerated ion beam. Even though the majority of the beam consists of protons, as mentioned above, we have been able to efficiently accelerate heavier ions (see section 3.3).

Up to now no measurement of the initial ion beam pulse duration has been performed, but based on the finite lifetime of the hot electrons a maximum pulse duration of a few picoseconds

has been concluded. Given the absolute numbers of ions (10^{13} protons at experiments using 1 PW lasers [2], 10^{12} protons at the LULI 100 TW system) the resulting initial ion beam current ranges in the mega-ampere regime.

The angular dependence of the energy distribution of the proton beam was measured with two ion spectrometers positioned at an angle of 0° and 13° , respectively. The measured spatial distributions of protons on the dispersion plane were deconvoluted (with respect to the entrance aperture shape) [9] and corrected for the spectrometer dispersion. A typical ion spectrum is shown in figure 2.

The energy of the protons emitted normal to the target rear surface extended up to 25 MeV. The maximum energy of the protons dropped to about 13 MeV at an angle of 13° , consistent with a two-dimensional model of the sheath acceleration process. The spectral shape of each proton energy distribution is generally continuous up to the cut-off energy, in agreement with the electrostatic sheath acceleration mechanism and as well as previous observations in experiments with the LLNL PETAWATT laser [2]. The best fit to the spectrum obtained by the ion spectrometers, as well as to the spectral information extracted from the stacked RCF packages was obtained by using a two component exponential distribution with 2 MeV and 6 MeV, respectively. Details about the angular dependence of the ion beam and the origin of occasionally observed narrow features in the spectral distribution, caused by the segregation of different ion species, are beyond the scope of this paper and will be published elsewhere.

For most of the future applications of laser generated ion beams the beam quality is the most important characteristic. Especially for the use as an ion source or the application as an inertial confinement fusion (ICF) ignitor beam, the ion beam emittance is crucial with respect to the accelerator structure acceptance or the achievable focus spot size. The formation of the ion beam is highly dependent on the formation of the electron sheath at the rear surface of the target (see section 3.2). We observed highly laminar and well collimated beams of ions using metal targets. As is apparent from the RCF data (see figure 3), the angular divergence of the proton jet is rather well defined and decreases with increasing proton energy. This suggests that protons or other light ions accelerated by this mechanism may have a useful small emittance in the sense of an actual ion beam.

To precisely estimate our emittance, we used penumbral imaging of edges at different distances from the target with the magnetic spectrometers, to directly measure the core emittance of the proton beam. This technique is closely related to the conventional slit-emittance measurements made with apertures and screens at conventional accelerators. We determine the normalized emittance of protons from flat gold foils to be $\sim 0.2\pi$ mm mrad, and factor of at least two smaller than the resolution limited measurements we performed on the

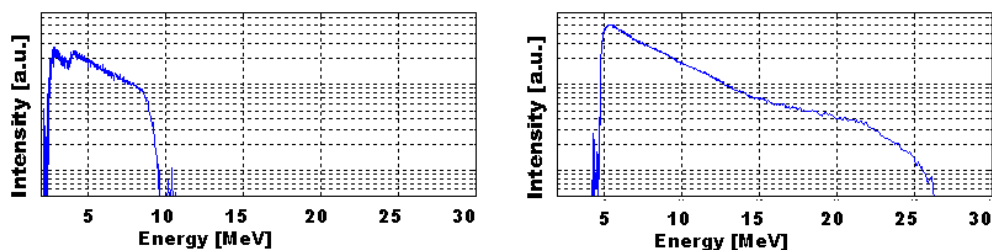


Figure 2. Typical proton spectra obtained at 20 J/350 fs pulses. Whereas the proton maximum energy extends up to 25 MeV normal to the rear surface (right), the maximum energy drops to below 10 MeV at an angle of 13° normal to the surface (left).

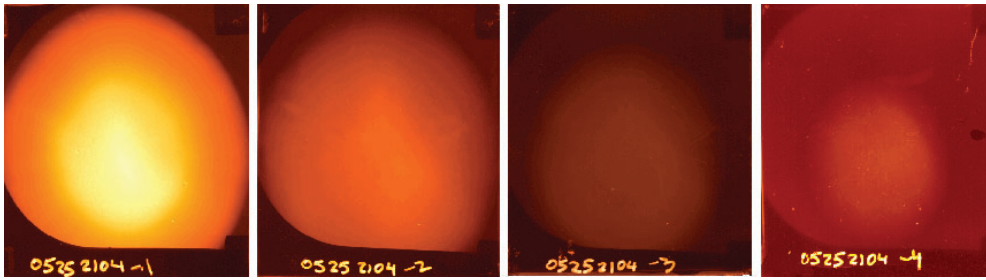


Figure 3. RCF images of the laser accelerated proton beam 5 cm behind the target. The ion energy increases from left to right. The divergence of the homogeneous beam decreases with increasing ion energy.

LLNL PETAWATT (see [2]). Details of the present measurements, and systematics of the proton emittance versus energy will be reported elsewhere.

The results of this analysis and subsequent modelling, developing a two-dimensional extension of the model in [10], suggest that we observe a rather cold proton beam, which is smoothly diverging and highly laminar. The trace space of the highest energy protons exhibits a tilted ellipse, whose width ultimately is the characteristic of the ion temperature. From these data, we deduce that the proton temperature is less than ~ 1 keV. From simple electron–ion collisional heating during the expansion, one may expect the ion temperature to be even lower, of order ~ 100 eV.

Using a newly developed technique that will be published in detail in [11] we have been able to improve the measurement of the beam core emittance by an order of magnitude. These measurements result in a transverse beam emittance of 0.06π mm mrad, which is orders of magnitude lower than achieved at any conventional accelerator.

It is interesting to note, that this measured beam emittance correspond to an effective ion temperature of less than 100 eV. This temperature is not consistent with the high temperatures present at the front surface, but likely maintained at the rear surface during the acceleration.

Moreover, one should be aware of the fact, that determining the source size by penumbral imaging techniques is misleading. The results obtained by this technique indicate spot sizes in the order of $10\text{--}20\ \mu\text{m}$. These spot sizes have been used in recent publications [12] to rule out the rear surface contaminants as the origin of the intense beams observed. However, in case of a highly laminar acceleration as expected for the TNSA mechanism the use of penumbral imaging traces back the virtual source size in the sense of a beam waist (as been reported at several conferences), which can be more than an order of magnitude smaller than the real source size at the rear surface. Recent experiments using direct surface imaging (see section 3.4) indicate the real source size to be much larger than the values obtained by penumbral imaging techniques.

Figure 4 shows the origin of the laser accelerated protons with respect to their energy. Protons up to energies of 3 MeV were emitted from an area of about $300\ \mu\text{m}$ diameter, far larger than the initial spot size at the front surface. The emission region decreases for higher energetic protons, in this case down to about $80\ \mu\text{m}$ for 10 MeV protons. The measurement is consistent with an electron sheath distribution caused by the higher electron density in the central region as predicted by numerical simulations [7, 8].

Recently, experiments at the LULI laser system using imaging techniques to determine the electron distribution at the target rear surface [13] show an excellent agreement between the electron distribution and the real proton source size at the target rear surface.

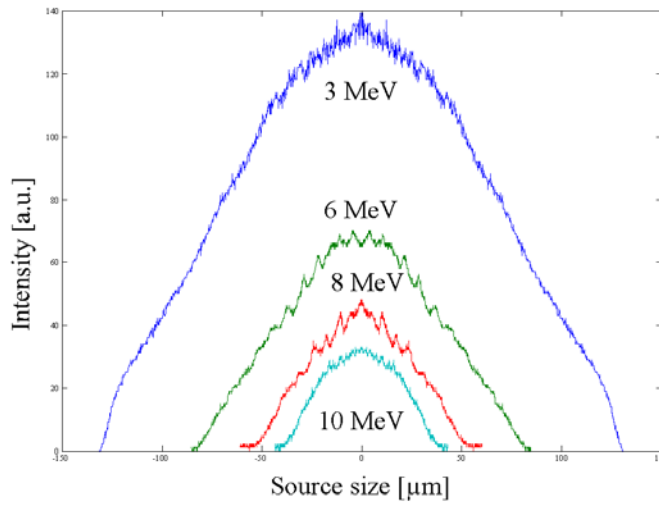


Figure 4. Real source size of the laser accelerated protons for different proton energies. The size at the rear surface decreases from $260\ \mu\text{m}$ for 3 MeV protons to $80\ \mu\text{m}$ for 10 MeV protons.

3.2. Target dependence

One of the interesting features of the laser accelerated ion beams is that their directionality is always normal to the rear surface of the irradiated target. Because of the small extension of the accelerating electron sheath and the strong dependence of their formation, target properties like the rear surface structure and target conductivity should have a major influence on the ion beam properties.

We have therefore performed detailed experiments to investigate the ion beam properties in dependence of these target parameters. In contrast to the homogeneous spatial distribution of protons originating from highly conducting (gold, aluminium) targets with a flat rear surface, ion beams emitted from targets with structured rear surfaces showed a strong filamentation. This effect could be explained by the presence of microfocusing filaments from these surface, as published in [14]. Furthermore, as expected from the TNSA mechanism, the scale length of the plasma at the rear surface is crucial for an effective ion acceleration. A large extension of a plasma at the rear surface has been shown to suppress the acceleration mechanism effectively [5, 15].

The formation of the accelerating sheath is dependent on the transport of the large electron currents through the target, thereby influenced by the onset of compensating return currents and effected by instabilities. The transport of relativistic electrons through the target is an extensively studied area of research [16–19] because of its relevance not only for ion acceleration, but especially for the concept of fast ignition [20–22] in ICF. It has been shown [2] that proton beams emitted from plastic targets always showed a filamentary structure. We used plastic and glass targets of varying thickness as well as layered targets to examine the influence of the target conductivity. Figure 5 shows a comparison of a simulation with the experiment for a $50\ \mu\text{m}$ plastic target coated with $10\ \mu\text{m}$ gold at the front surface. The left part of the figure shows the accelerating electron sheath assuming electron beam breakup into three large filaments during the propagation in the target. The central part of figure 5 presents the simulated ion beam structure at the location of our detector several cm behind the target. This is compared to the experimental data shown in the right part of figure 5. As can be seen,

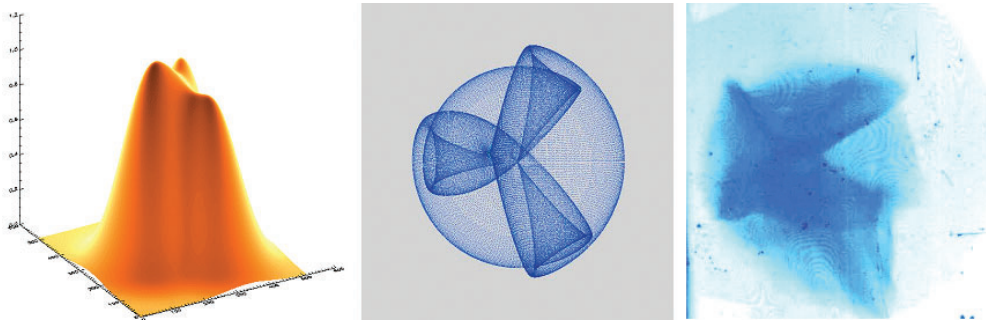


Figure 5. Proton beam filamentation due to electron transport. Simulation of a filamented electron sheath (left) in plastic causes the proton beam to show structure (central part). The experiment (right) shows an excellent agreement with the simulation.

there is an excellent agreement between the simulated beam pattern to the experiment which indicates electron beam breakup to be the origin of the beam filamentation. Similar results have been obtained using targets coated with conducting layers at the front and the rear surface.

3.3. Heavy ion acceleration

So far mainly protons have been observed from the rear side, originating, as in the long-pulse experiments, from contaminating hydrocarbon layers which coat the targets. As soon as protons are present they outrun the heavier ions and screen the acceleration field. We present the first experimental study, demonstrating that besides protons, also high-quality, high energy (\sim MeV/nucleon) heavy ion beams can be accelerated from the rear surface of (coated) thin foils. We find that heavy ions are effectively accelerated, provided the hydrogenous surface contaminants are removed. We obtained high resolution, absolutely calibrated energy spectra of different ion species, which provide additional information, not available in the proton signal, about the spatio-temporal evolution of the accelerating field and the origin of the observed ions. Details on the acceleration of heavy ions are to be published in [23]. To effectively remove the hydrogen contaminants we resistively heated tungsten targets up to temperatures of 1000 K for several minutes. The ion species of interest was coated solely on the rear surface of the target, thereby unambiguously verifying the origin of the heavy ions. The proton spectrometer as well as the CR-39 did not show any protons, while strong fluorine ion tracks are observed originating from the CaF_2 layer at the target rear side. The complete removal of contaminants increased the acceleration of heavier ions considerably. Quantitative evaluation shows that F^{7+} was accelerated up to 100 MeV, i.e. more than 5 MeV/nucleon at 4% energy conversion. The RCF diagnostic confirmed this by showing a narrow spot in the first layer, which, in the absence of protons, indicates fluorine ions of energies above 4 MeV/nucleon. The evaluation of the fluorine shot shown in figure 6 shows that E -fields $E_{\text{stat}} \sim 2 \text{ TV m}^{-1}$ on a timescale of $\tau \sim 350 \text{ fs}$ are necessary to accelerate F^{7+} -ions up to 100 MeV over a scale length of $l \sim 10 \mu\text{m}$. The shot presented in figure 6 was virtually without any protons, but the modelled fields can accelerate protons up to $\sim 25 \text{ MeV}$, as typical with unheated targets. The field distribution is in agreement with an extended TNSA model including dynamic fields and multiple ion species. We found that field ionization is the dominant mechanism while recombination and collisional ionization are by far less effective (see [23]). Since the targets were coated only at the back surface and we successfully removed contaminations and can rule out front side acceleration within the parameters of our experiment.

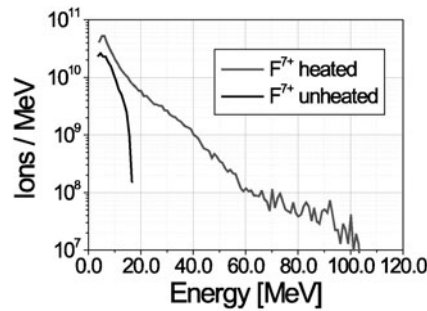


Figure 6. Heavy ion acceleration in the presence (unheated) and without (heated) proton contaminants. More than 100 MeV (5 MeV/nucleon) F^{7+} ions were measured.

3.4. Ion beam tailoring

An important question to be addressed for any future application of laser-accelerated protons and ions is the possibility of tailoring the proton beam, either collimating or focusing it, by changing the geometry of the target surface. Due to the excellent beam quality and the close correlation of the accelerating sheath to the rear surface tailoring of the ion beams should be feasible using appropriate target design. However, ballistic focusing of the laser accelerated protons is expected to be rather difficult because of the inherent divergence associated with the spatial variation of the density of the hot electron sheath, which drives the acceleration. Accordingly, we first attempted to de-focus the beam in one dimension, by using a convex target. Using a $60\ \mu\text{m}$ diameter Au wire as a target basically constituted such a one-dimensional de-focusing lens, and we observed a line image as published in [14]. Tilting the wire also changed the orientation of the line image, which results from the radial, fan-shaped expansion of the protons normal to the surface of the wire. We then attempted to focus the protons by modifying the curvature (concave) of the target foil. Due to the Gaussian-like shape of the hot electron Debye sheath that causes the acceleration, there is an energy dependent angle of divergence that has to be compensated to focus the ions in the energy range of interest. Therefore, the effective focal length of a curved target rear surface is longer and is dependent of the proton energy. The results, that will be published elsewhere show a strong reduction in the divergence of the central core of the proton beam representing ballistic collimating of laser produced proton beams.

Based on the excellent beam emittance that implies a highly laminar expansion of an initially very cold ion beam we investigated the prospect of imaging the actual target surface by means of the protons. This would further allow the precise determination of the real source size, details about the electron transport and has the prospect of many applications. Initial experiments showed substructures in the proton beam that could be related to surface structures at the μm scale. Figure 7 shows an image of a 50 mm gold target rear surface obtained by using a scanning electron microscope (SEM). Due to the fabrication process, elliptical structures (holes) at the surface remain at a diameter of a few μm . In the right part of the figure, we present typical substructures of the proton beam emitted from that surface. The shape of the structures in the beam resembles the structures at the surface. Meanwhile we have succeeded to use artificial surface structures, like lines, grids, crosses and names on a μm scale to tailor laser accelerated proton beams. The results will be published elsewhere [11], but the excellent quality of the beam allows to tailor ion beams with fiducial patterns, which is highly interesting for any imaging techniques, like proton radiography, or electrical field mapping.

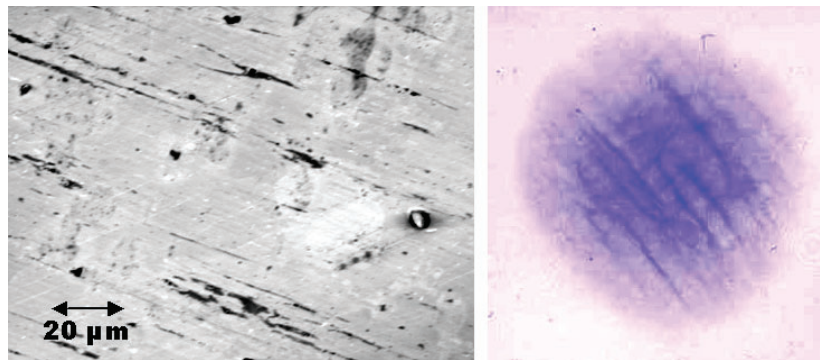


Figure 7. Surface imaging by laser accelerated protons. The structures at the target rear surface (SEM image, left) were imaged by the proton beam onto the detector (right).

4. Conclusion

Laser accelerated proton and ion beams offer new prospects for a whole variety of applications. The beam quality was found to be far superior to beams accelerated by conventional accelerators with respect to the transversal beam emittance, while the longitudinal phase space was found to be comparable. The beam intensity exceeds present accelerators by orders of magnitude. The excellent beam quality implies a highly laminar acceleration and an initially extremely cold beam and the experiments proved the beam to have optical qualities. The properties are highly interesting for applications, especially as we have shown the possibility of tailoring the beam with respect to shape, ion species, efficiency [14], and homogeneity. A wealth of applications are currently being investigated, starting from improved diagnostic capabilities [6], to industrial and medical applications, to next generation ion sources and prospects for fast ignition in inertial ICF [4, 24]. Still the underlying physics is subject to further investigation and, with respect to the extensive interest, future improvements are likely to be developed in the next years.

Acknowledgments

This work was supported by the EU Contract No. HPRI CT 1999-0052, and in part by grant E1127 from Region Ile-de-France.

References

- [1] Clark *et al* 2000 *Phys. Rev. Lett.* **84** 670
- [2] Snavely R *et al* 2000 *Phys. Rev. Lett.* **85** 2945
- [3] Wilks S C *et al* 2001 *Phys. Plasmas* **8** 542
- [4] Roth M *et al* 2001 *Phys. Rev. Lett.* **86** 436
- [5] Roth M *et al* 2002 *PRST-AB* **5** 061301
- [6] Borghesi M *et al* 2001 *Plasma Phys. Control. Fusion* **43** A267
- [7] Ruhl H *et al* 2000 *Plasma Phys. Rep.* **27** 363
- [8] Pukhov A 2001 *Phys. Rev. Lett.* **86** 3561
- [9] Lucy L B 1974 *Astron. J.* **79** 745
- [10] Wickens L M and Allen J E 1981 *Phys. Fluids* **24** 1984
- [11] Cowan T E *et al* *Nature* submitted
- [12] Zepf M *et al* 2001 *Phys. Plasmas* **8** 2323

-
- [13] Santos J J *et al* 2000 Rapport LULI 2000, p 19
 - [14] Roth M *et al* 2002 *AIP Conf. Proc.* vol 611, ISBN 0-7354-0057-1, p 199
 - [15] MacKinnon A J *et al* 2001 *Phys. Rev. Lett.* **86** 1769
 - [16] Haines M G 1981 *Phys. Rev. Lett.* **47** 917
 - [17] Key M H *et al* 1998 *Phys. Plasmas* **5** 1966
 - [18] Malka G and Miquel J L 1996 *Phys. Rev. Lett.* **77** 75
 - [19] Beg F N *et al* 1997 *Phys. Plasmas* **4** 447
 - [20] Tabak M *et al* 1994 *Phys. Plasmas* **1** 1626
 - [21] Deutsch C *et al* 1996 *Phys. Rev. Lett.* **77** 2483
 - [22] Batani D *et al* 2000 *Phys. Rev. E* **61** 5725
 - [23] Hegelich M *et al* 2002 *Phys. Rev. Lett.* **89** 085002
 - [24] Atzeni S *et al* 2001 *Proc. 28th EPS Conf. on Contr. Fusion and Plasma Physics (Madeira, 2001)*